Supporting Materials and Methods

Anatomical methods

Tracer Injections and Tissue Processing. To define multi-synaptic afferents to VTA, we used pseudo-rabies virus (PRV), a retrograde transynaptic tracer that has been used in several studies to help delineate multisynaptic circuit projections *(S1, S2)*. Brain tissue from animals used in a previous study *(S3)* were additionally processed, or re-examined for purposes of the current study. Details on surgical procedures, immunohistochemical processing, and schematics of injection sites are described in Luo and Aston-Jones (2009).

In brief, 29 adult male rats Sprague Dawley rats (250-415 g) were used. All housing and surgical procedures conformed to the BioSafety level II regulations for studies involving the use of infectious pathogens [United States Department of Health and Human Services Publication (Centers for Disease Control and Prevention) No. 88-8395; *Biosafety in Microbiological and Biomedical Laboratories*)], and were approved by the University of Pennsylvania Institutional Animal Care and Use Committee in accordance to the National Institutes of Health specifications outlined in the Guide for the Care and Use of Laboratory Animals.

For tracer injections, a mixture of PRV (Bartha strain; 1.7 x 109 pfu/ml of culture media) *(S4)* and cholera toxin subunit B (CTb; 0.05% in dH20) was unilaterally injected into VTA through glass micropipettes (30-35 μm diameter tip) using brief pneumatic pulses from a Picospritzer controlled pressure source. CTb was included in the injection solution to localize injection sites because PRV is avidly taken up and transported away by terminal afferents. Because of the large size of PRV virions, injected CTb diffuses more than PRV, and therefore likely over-estimates the actual spread of injected PRV *(S5)*. Inclusion of CTb also helped differentiate between direct and indirect afferents. A volume of 480 nl of PRV/CTb was empirically found to give adequate transport while maintaining focal injection size. For lesion studies (n = 8 animals), ibotenic acid was injected bilaterally into caudodorsal-lateral septum (cd-LS; 300 nl each hemisphere; similar method as with PRV/CTb injections) 5-7 days before PRV/CTb injection in VTA.

Because PRV's multisynaptic replication and transport occurs in synaptically-linked circuits in a time-dependent manner *(S4)*, a time-course analysis of PRV retrograde labeling after injection into VTA was performed. Animals were sacrificed 24, 36, 48, 52, 60, or 72 h post-injection (n = 2, 4, 5, 3, 5, and 2 animals at each respective time-point). Although time-dependent labeling with PRV is a highly effective means of characterizing the hierarchy of afferent circuitry, time-course analysis alone does not allow conclusions regarding the number of synapses (relays) within the pathway.

Animals were deeply anesthetized and transcardially perfused with 4% paraformaldehyde. Brains were cryoprotected in 20% sucrose and cut into 40μm-thick coronal sections using a cryostat, and collected in polystyrene Multidishes such that each well consisted of the entire brain at 240 μm intervals. Tissue sections were immunohistochemically processed using an avidin-biotin-horseradish peroxidase complex method, and then visualized by incubation in a 3,3-diaminobenzidine solution with or without ammonium nickel sulfate, or in Vector SG substrate. The following primary antibodies were used: (1) polyclonal rabbit anti-PRV antibody (1:5000, DP 134; gift from R. Miselis ; (2) polyclonal goat anti-CTb (1:10,000); (3) monoclonal mouse anti-NeuN (1:1000); and (4) monoclonal mouse anti-TH (1:6000). Methyl Green was used to counterstain tissue sections.

Cell Quantification. Brain section-mounted slides were examined using a microscope, and photomicrographs were acquired using a digital camera, or film scanner. Stereo-Investigator was used to quantify PRV and/or NeuN (+) neurons. For hippocampus, previously established boundaries for dorsal, intermediate and ventral subregions were used *(S6)*, with the intermediate CA3 predominate from approximately -5.0 to -5.6 mm to bregma, although dorsal and ventral CA3 are also present at these rostral-caudal levels. PRV (+) neurons were cataloged accordingly (e.g., neurons in the ventral aspect of CA3 in a coronal section at approximately -5.3 mm from bregma were categorized as ventral CA3

neurons). The small region between CA1 and CA3 classically termed CA2 is often grouped with CA3, as was done in the current study. Sections at 480 µm intervals throughout Ammon's horn were counted. For lateral septum, previously established boundaries for dorsal, intermediate and ventral sub-regions were used *(S7)*. We further divided lateral septum into rostral and caudal sub-regions, with the rostral pole of bed nucleus of the stria terminalis (approximately +0.5 mm to bregma) serving as the boundary between the two regions. Sections at approximately 240 µm intervals throughout lateral septum were analyzed. Using the Stereo-Investigator Contour tool, regions of interest were first selected. PRV or NeuN (+) neurons within the regions of interest were counted using the Marker tool, so that no cells were counted twice, and the total number of counted cells was automatically displayed.

Electrophysiological Methods

Animals. Fifty-two male Sprague-Dawley rats (275-415 g) were used. Animals were housed two to three per cage under controlled conditions (22-23°C; 12/12 light-dark cycle, lights on 7am) with food and water available *ad libitum*. All procedures were approved by the Institutional Animal Care and Use Committee of the National Institute of Drug Abuse Intramural Research Program in accordance to the National Institutes of Health specifications outlined in the Guide for the Care and Use of Laboratory Animals.

Surgery. Animals were anesthetized with urethane (1.4 g/kg) and placed in a Kopf stereotaxic frame large enough to accommodate multiple stereotaxic electrode carriers simultaneously. Body temperature was maintained at 37°C using a thermistor-controlled heating pad. Electrodes and/or ejection pipettes were placed in dorsal CA3 hippocampus, caudodorsal-lateral septum (cd-LS), ventral subiculum (vSUB), lateral ventricle, or ventral tegmental area (VTA). All anatomical sites were in the hemisphere ipsilateral to VTA recording sites. Given the geometric complexity of orienting multiple stereotaxic electrode carriers, the stereotaxic coordinates (with flat skull) for targeted anatomical sites are listed: 1) dorsal CA3: -3.0 mm from bregma, 3.4 mm from midline, 3.5-3.8 mm from skull, 2) cd-LS: +0.35 mm from bregma, 0.6 mm from midline, 4.2 mm from skull, 3) vSUB: -5.5 mm from bregma, 3.8 mm from midline, 8.4 mm from skull, 4) lateral ventricle: -0.3 mm from bregma, 1.2 mm from midline, 3.6 mm from skull.

Electrical Stimulation of dorsal CA3. Forty-two rats received electrical stimulation of dorsal CA3. A concentric, bipolar, stainless steel electrode (250 µm overall diameter, with 100 µm tip separations) was lowered into dorsal CA3. Electrical stimuli were generated by CED 1401-Spike2 software and an ISO-Flex stimulus isolation unit. Two stimulation patterns were used; single-pulse and theta frequency. When possible, cells were tested for both types of stimulation patterns. Single-pulse stimulation consisted of 0.5 mA, 0.3 ms pulses delivered at 2 s intervals, repeated 40-80 times per cell, similar to previous studies *(S8)*. Theta frequency stimulation consisted of pulses (0.5 mA, 0.3 ms) delivered in 20 high-frequency bursts (5 pulses at 100Hz), separated by theta frequency intervals (200 ms), consistent with previous studies *(S9, S10)*. Theta train stimulation was only applied 1-3 times per recorded cell, with an inter-train interval of at least 2 minutes, to minimize the induction of synaptic plasticity.

Drug microinjections. Ejection pipettes consisted of glass micropipettes with tip diameters 35-45 µm filled with one of the following drugs: 1) 1.0 M GABA in aCSF, 2) 1.0 mM D,L-homocysteine (DLH) in aCSF, or 3) mixture of 0.5-1.0 mM picrotoxin and 0.2-0.4 mM CGP55845 in aCSF. The concentrations of GABA *(S11)*, picrotoxin and CGP55845 *(S12)* were consistent with previous studies of *in vivo* DA neuron impulse activity. The concentration of DLH (1.0mM) was empirically derived through pilot studies aimed at achieving consistent activation of CA3 pyramidal cells without inducing depolarization block (see Fig. S7). Drugs or vehicle (aCSF) were ejected by brief pulses of pneumatic pressure. At least 45 min separated any two drug infusions. For inactivation tests via GABA infusion, VTA neuron baseline responses to dorsal CA3 stimulation was first established, and then approximately 240 nl of GABA was slowly microinjected into the cd-LS (Fig. S1; $n = 8$ animals) or vSUB ($n = 8$ animals) hemisphere ipsilateral to the VTA recording site. Dorsal CA3 was then stimulated every 2-4 min until

either the baseline response was recovered or a stable cell recording could no longer be maintained (up to 30 min). A similar protocol was used for picrotoxin-CGP 55845 tests (n = 7 animals), except that 30 nl of the drug mixture was microinjected via a double-barrel micropipette *(S8)*. For CA3 chemical stimulation studies, CA3 pyramidal neurons were first recorded using the same double-barrel micropipette configuration to optimize the injection protocol of 60 nl of DLH (n = 4 animals). In subsequent tests, 60 nl of DLH was released in CA3 via a single-barrel micropipette (Fig. S6) while recording VTA neuron impulse activity (n = 10 animals).

Neuronal Recordings. Single-unit, extracellular recordings were obtained using a glass micropipette (8-12 MΩ) filled with a 2.0% pontamine sky blue solution in 0.5M sodium acetate. For juxtacellular labeling, a glass micropipette (12-20 MΩ) filled with 4.0% Neurobiotin in 0.5 M potassium acetate was used. In some cases, double-barrel micropipettes were custom fabricated as previously described *(S8)*, to allow simultaneous VTA or CA3 pyramidal neuron recordings with local microinjection of drugs (e.g., picrotoxin & CGP 55845) via Picospritzer. Electrophysiological signals were amplified and filtered (0.2-10 kHz bandpass) using a pre-amplifier and amplifier in bridge mode. Data were acquired and stored on a computer using a hardware-software interface system. Only spontaneously active VTA neurons were recorded and analyzed. Neurons were recorded for 3-5 min to establish a mean baseline firing rate. VTA recordings were obtained from each animal using a sampling grid that extended 0.4-1.2 mm from midline, 7.0-9.0 mm from brain surface, and 4.8-6.2 mm caudal to bregma. The electrode carrier was angled 10° from midline to improve access to medial aspects of VTA without disrupting the vasculature of the central sinus. The electrophysiological properties used to tentatively identify the neurochemical subtypes of VTA neurons were similar to previous studies *(S13-S15)*. In brief, the initial spike duration of a waveform was calculated from the start of the action potential to the peak of the negative trough. Putative DA neurons were defined as having initial spike durations ≥ 1.1ms and mean firing rates < 10 spikes/sec. Putative GABA neurons had initial spike durations < 1.1ms and mean firing rates > 10 spikes/sec. For DLH optimization studies, CA3 pyramidal neurons were identified by previous electrophysiological characteristics *(S16)*. For electrical stimulation studies, an average of 4.0 ± 0.4 VTA neurons per animal was recorded for analysis; for chemical stimulation studies an average of 4.2 ± 0.5 VTA neurons was recorded per animal.

Histological verification. At the end of an experimental session, recording and drug ejection sites were histologically marked. For CA3 electrical stimulation sites, constant current (0.5 mA, 5 s) was used to mark the area. For drug ejection sites (i.e. GABA or aCSF in cd-LS or vSUB, and DLH in CA3), the ejection pipette was carefully replaced at the same stereotaxic location, with a micropipette filled with either 2% evans blue or 2% pontamine sky blue. Sixty nl of evans blue was pressure injected via Picospritzer, or in the case of pontamine sky blue, iontophoresed (-20 µA for 10-12 min). For non-perfused animals, brains were removed and snap-frozen in a -70°C solution of methyl butane. Coronal, 40 µm-thick sections of brain were cut on a cryostat and counterstained with fast red.

Immunohistochemistry for juxtacellularly labeled neurons. At the end of recording experiments with juxtacellular labeling, animals were perfused with 0.9% NaCl followed by 4% paraformaldehyde in 0.1M phosphate buffer. Brains were post-fixed overnight, and transferred to an 18% sucrose-0.1M phosphate buffer solution. Coronal sections of brain were cut at 40 µm intervals on a cryostat. Sections at approximate rostral-caudal levels of VTA were collected serially in a 24-well plate, 3-5 sections per well, with sections in each well approximately 400 µm apart to aid in rostro-caudal realignment during slide mounting. Free-floating sections were incubated in 0.03% hydrogen peroxide/0.1M phosphate buffered saline (PBS) solution for 15 min, followed by an incubation in 2% normal donkey serum - PBS solution for 2-6 h. Sections were then incubated overnight in a polyclonal mouse antibody to tyrosine hydroxylase (TH, 1:1000) - 2% normal donkey serum - PBS-0.3% triton solution. Sections were then incubated in an Alexa Fluor 594 nm-conjugated donkey anti-mouse antibody (1:100), and Streptavidin Alexa Fluor 488 nm (to reveal neurobiotin-labeled cells; 1:400) - 2% normal donkey serum - PBS-triton solution for 2 h.

Between all incubations, sections were rinsed 3 times, 10 min each in PBS. Sections were mounted onto coated slides and coverslipped with Slowfade anti-fade mounting solution.

Data Analysis. For single pulse stimulation studies, cumulative peristimulus time histograms (PSTHs; 5 ms bins) were generated and analyzed for inhibitory and excitatory epochs similar to previous studies *(S8)*. These metrics produced a response latency, duration and magnitude. Briefly, baseline was defined as the 500 ms epoch prior to stimulation. The onset of excitation was defined as the first of 5 consecutive bins whose mean value exceeded mean baseline activity by 2 standard deviations. The onset of inhibition was defined as the first of at least 15 bins whose mean value was at least 35% below baseline. Responses were normalized by the following equation to produce a response magnitude (Rmag):

R-mag = (# of spikes in response epoch) – [(mean # of spikes per baseline bin) * (number of bins in response epoch)]

During theta train stimulation, we noticed that some VTA neurons had qualitatively different responses early vs. late post-stimulation. Therefore, we defined early and late epochs and quantified responses during these epochs. Based on the response during the early and late epochs, each tested neuron was assigned to a two-letter category, with the first letter representing the direction of the response during the early epoch: "I" for inhibition, "E" for excitation, and "N" for non-responsive. For example, a neuron respond with early inhibition followed by late excitation would be designated "I-E".

The early epoch was defined as the time period from the onset of stimulation to 5 s post-stimulation [early epoch = 3.9 s (stimulation) +5.0 s (post-stimulation) = 8.9 s). The late epoch was defined as the time period from 5 to 60 s post-stimulation. Because of possible spike occlusion during high frequency (100 Hz) stimulation artifacts, we lacked the fine resolution to accurately determine response onset. Responses during the early epoch were quantified and normalized by the following equation to produce a response score (R-score) where Baseline epoch was defined as the 8.9 s prior to stimulation, the same time period as the Early epoch.

R-score = (# of spikes in Early epoch) / [(# of spikes in Baseline epoch) + (# of spikes in Early epoch)]

The R-score range was from 0.0 to 1.0 with 0.5 defined as "no change". Threshold for excitation and inhibition were defined as Rscores > 0.55 or < 0.45, respectively. This R-score deviation corresponds to an approximately 20% increase or decrease, respectively, in firing rate over baseline. A cell's late epoch response was analyzed by statistically comparing its interspike-interval histogram (ISIH; 5 ms bins) to its baseline epoch (60 s pre-stimulation) ISIH. Cells were considered responsive if the two ISIHs were different by Kolmogorov-Smirnoff, with the alpha level set at 0.01. For analysis of time-courses for neuronal responses (i.e., Fig. 2C), spikes were re-analyzed in 10 s bins from 60 s pre-stimulation to 180 s post-stimulation.

Firing rate (spikes/s), coefficient of variation (standard deviation/mean ISI), and percentage of spikes in burst (SIB) were also calculated. The onset of a burst was defined as at least two spikes occurring with an inter-spike interval < 80ms *(S14, S17)*. The percentages of spikes in bursts were calculated by dividing the numbers of spikes occurring in bursts by the total numbers of the spikes in the same time periods. The percentages of spikes in burst were only calculated for putative DA neurons. For chemical stimulation tests with DLH, we compared ISIHs (5 ms bins) during three time periods: pre-drug (180 s), during-drug (160 s), and post-drug (180 s). ISIHs during each time-period were compared by a Kolmogorov-Smirnov test (alpha level = 0.01), and neurons were considered responsive if their during-drug and/or post-drug firing activity was significantly different from pre-drug.

Behavioral Methods

Animals. Thirty-four naive male Sprague-Dawley rats (300-350 g at time of surgery) were individually housed in a temperature- and humidity-controlled animal facility at the Medical University of South Carolina (MUSC) under a reversed 12-h light/dark cycle (lights off at 6 a.m.), with *ad libitum* access to food and water. All experiments were approved by the Institutional Animal Care and Use Committee at MUSC in accordance to the National Institutes of Health specifications outlined in the Guide for the Care and Use of Laboratory Animals.

Surgery. Construction of chronic indwelling catheters and catheter surgeries were done as described previously *(S18)*. In brief, a week after acclimation to the animal facility, rats were anesthetized with ketamine/xylazine (66.6/1.3 mgkg-1, i.p.); a non-steroidal anti-inflammatory drug (meloxicam) was also administered prior to surgery. The free end of the catheter was inserted into, and secured to the right jugular vein. The other end was passed subcutaneously over the right shoulder, exiting a biopsy hole between the rats' shoulders, and mounted on the back. Stereotaxic surgery followed immediately after the catheter surgery. For intracerebral drug or vehicle infusions, rats were implanted with bilateral 26G guide cannulae aimed 1 mm above CA3 (-3.45 mm from bregma, ± 3.55 mm from midline, and 3.0 mm from skull), or unilaterally 2 mm above LS and contralateral VTA. LS and VTA-directed cannulae were angled 10º away from midline to avoid vasculature. The same anatomical sites were targeted as in electrophysiological studies, but to account for the additional 10º angle, the following coordinates were used: LS, +0.2 mm from bregma, ±1.63 mm from midline, -2.8 mm from skull; VTA, -5.6 mm from bregma, ± 2.2 mm from midline, -7.1 mm from skull. Implanted cannulae were secured to the skull using four jewel screws and dental cement. To prevent infection and occlusion, tips of i.v. catheters and cannulae were covered by stylets and caps. The tips of inner injection 30G cannulae extended 1 mm (for CA3) or 2 mm (for cd-LS and VTA) below the guide cannulae into the injection sites. Animals were given 1 week to recover from surgery before behavioral studies. From post-surgery day 3 until the last self-administration session, catheters were flushed daily with 0.1 ml each of the antibiotic cefazolin (100 mg/ml) and heparin (100 U/ml). Prior to each self-administration session, catheters were also flushed with 0.1 ml saline to ensure patency.

Behavioral experiments. Self-administration started one week after surgery. All behavioral experiments were conducted during the dark (active) cycle. The ABA reinstatement paradigm was similar to our previous work *(S18)* with minor modifications. Briefly, using a combination of different visual, auditory, olfactory, and tactile cues, two distinct self-administration environments were created in the operant chambers: context A consisted of 2 s on/2 s off tone cues (78 dB) and a flashing white light above the active lever, lemon odor, and a grid floor; whereas context B consisted of a continuous red house light opposite to the operant levers, continuous white noise, vanilla odor, and metal mesh flooring. Intravenous self-administration and delivery of visual and auditory cues were controlled by a MED-PC IV program. Rats were randomly assigned to learn active lever-pressing for i.v. cocaine (Fixed Ratio-1) in either context A or B during daily 2 h sessions until they reached the criteria of 10 self-administration sessions with > 10 infusions / 2 h. Presses on an inactive lever had no programmed consequences. Acquisition of cocaine self-administration is shown in Fig. S2. Rats then experienced daily 2 h extinction sessions in the alternative context (B for A animals, A for B animals), during which presses on either lever had no consequences (no drug), until they met the criteria of two consecutive sessions with < 25 active lever presses (minimum of 7 sessions prior to the first reinstatement test; minimum of 2 sessions between subsequent reinstatement tests). A sham injection (insertion of injection cannulae without infusion; 1 or 2 mm above the tip of guide cannulae for CA3 or LS-VTA, respectively) was done prior to the last extinction session to serve as a control and to adapt rats to the intracranial infusion. Following extinction training, two 2 h context-induced reinstatement tests (separated by a minimum of 2 extinction sessions with < 25 active lever presses) were conducted during which animals were returned to their previously cocaine-paired context. To assess the effect of inactivating brain regions of interest on reinstatement of

cocaine-seeking, separate groups of animals received either bilateral inactivation of dorsal CA3 (n = 8 animals) or asymmetrical inactivation of cd-LS and VTA (n = 14 animals) by infusing a mixture of the GABA-B and GABA-A receptor agonists, baclofen and muscimol (B-M) into these respective brain regions in contralateral hemispheres (Fig.S3). The injection cannulae were left in place for 90 s after the infusion and the reinstatement test began 5 min after removal of the injector. During the reinstatement sessions, presses on either lever had no consequences. The concentrations and volumes of B-M injections for CA3 and LS were 1.0 mM baclofen and 0.1 mM muscimol (0.5 µl / hemisphere / brain region), and for VTA were 0.1 mM baclofen and 0.01 mM muscimol (0.3 µl), or aCSF in the same volumes. These concentrations and volumes used in reinstatement tests were based on previous behavioral studies in dorsal hippocampus *(S19)* or empirically derived from the locomotion studies. These locomotor tests were conducted to rule out possible effects of intracranial infusions of B-M on motor activity, and consisted of continual monitoring of horizontal and total activity during a 2 h session in an open field apparatus, in rats receiving bilateral CA3 (n = 5) or contralateral LS-VTA (n =12) infusions.

At the end of behavioral studies, rats were euthanized with an overdose of ketamine and xylazine, and pontamine sky blue dye was infused (0.5, 0.5, and 0.3 µl into the CA3, LS, and VTA, respectively) for subsequent histological verification.

Statistical Analysis. Results are expressed as the mean ± SEM, unless otherwise noted. All data sets were first tested for normality to determine the use of parametric or non-parametric statistical tests. The following parametric tests were used, as appropriate: Unpaired and paired t-tests, Kolmogorov-Smirnov (K-S) test, one-way and factorial ANOVA followed by Newman Keuls post-hoc test, and repeated measures ANOVA followed by Dunnett's or Bonferroni post-hoc tests. The following non-parametric tests were used, as appropriate: Mann-Whitney (M-W), Kruskal-Wallis (M-W) followed by Dunn's post-hoc test. Contingency tables were analyzed by a Fisher Exact test. The alpha level was set 0.05 unless otherwise noted.

Supporting Text

PRV labeling in intermediate and ventral CA3. Beginning at 48 h after injection of a PRV and cholera toxin B subunit (CTb) mixture into VTA (Fig. S4A), PRV (+) neurons were consistently found in intermediate (Fig. S4B) and ventral (Fig. S4E) hippocampus in addition to dorsal hippocampus as described in main text (Fig. 1). The pattern and time-course of PRV labeling in intermediate, and ventral hippocampus were similar as that in dorsal hippocampus; labeling was first observed at 48 h post-injection, and was bilateral and restricted to the CA3 pyramidal cell layer. For both intermediate and ventral hippocampus, PRV labeling tended to be lateralized; that is, more PRV (+) neurons were found in ipsilateral intermediate and ventral CA3 than their respective contralateral hemispheres, although this difference was not significant (Fig. S4D, E, and F; factorial ANOVA, Newman-Keuls *post-hoc*; intermediate; ipsilateral, 99.0 ± 18.8 vs. contralateral, 59.8 ± 12.3; P=0.52; ventral, ipsilateral, 95.9 ± 11.2 vs. contralateral, 53.4 ± 12.5, P = 0.60).

PRV labeling in hippocampus at 60 h post-injection. By 60 h post-PRV injection in VTA, dorsal, intermediate, and ventral CA3 cell fields were each heavily labeled with PRV (+) neurons (dorsal and intermediate fields are shown in Fig. S5; a similar pattern was observed in the ventral field). Additional hippocampal cell areas also exhibited labeling, consistent with time-dependent retrograde transport of PRV. Labeling was observed in dentate gyrus cells, an area known to project to the CA3 pyramidal cell layer via the mossy fiber pathway (Fig. S5A). Stratum oriens horizontal cells, which project exclusively to pyramidal cells *(S20),* were also labeled (Fig.S5B, right). Notably, labeling was still absent in vSUB, as mentioned in main text (Fig. 1C). We observed apparent necrotic cells which tended to cluster in the CA3b subregion of the CA3 pyramidal cell layer (delineated by yellow arrowheads in Fig. S5A, left and S5B, right). Because PRV is eventually lethal to infected neurons *(S4)*,

these necrotic-like neurons were likely infected with PRV at an earlier time-point than non-necrotic neurons. Therefore, it is possible that these CA3b pyramidal cells were the initial hippocampal neurons labeled with PRV in our study.

Intermediate and ventral CA3 not likely part of the hippocampus to cd-LS to VTA circuit projection. Lesions of cd-LS resulted in non-significant changes in the mean number of PRV (+) cells in ipsilateral and contralateral intermediate and ventral CA3. When dorsal, intermediate and ventral subregions were analyzed using a factorial ANOVA design, there was a main effect of the lesion on the overall number of PRV (+) neurons, but *post-hoc* analysis revealed that lesions of cd-LS did not significantly change the number of PRV (+) cells in either the ipsilateral intermediate (Fig. S4D, E and F; intact, 99.0 ± 18.8 vs. lesioned, 53.4 ± 11.2; Newman-Keuls *post-hoc*, $P = 0.43$), contralateral intermediate (intact, 59.8 ± 12.3 vs. lesioned, 79.4 ± 21.2; $P = 0.80$), ipsilateral ventral (intact, 95.9 ± 15.6 vs. lesioned, 43.5 ± 15.9; $P = 0.65$), or contralateral ventral (intact, 53.4 ± 12.5 vs. lesioned, 71.3 ± 18.1; $P = 0.69$). That cd-LS did not significantly change the number of PRV (+) neurons in either intermediate or ventral CA3 is not surprising, as the CA3 projection to LS is topographical. Thus, the dorsal (septal) to ventral (temporal) organization of CA3 pyramidal cells is maintained in its projection to LS; dorsal CA3 pyramidal cells project to dorsal LS, whereas intermediate and ventral CA3 pyramidal cells tend to project to intermediate and ventral LS, respectively *(S21)*. This dorsal-ventral gradient may explain, in part, why there was a decrease, albeit non-significant, in the number of PRV (+) neurons in the ipsilateral intermediate and ventral CA3 in cd-LS lesioned animals. There tended to be an increase in PRV (+) neurons in contralateral intermediate and ventral CA3 in cd-LS lesioned animals, although the differences, as mentioned above, were not significant (Fig. S4D). The mechanism and possible functional importance of this increase in the number PRV (+) neurons in the contralateral hemispheres in cd-LS lesioned animals is unclear.

It is currently unknown how PRV virions were retrogradely transported to intermediate and ventral CA3 as we observed little labeling of intermediate lateral septum and even less in ventral lateral septum at 36 h (Fig. 1D). One possibility is *via* the vertical limb of the diagonal band (vDB). The vDB is a known afferent to VTA *(S22, S23)* and also receives projections from ventral, but not dorsal CA3, leading us to speculate that ventral CA3 labeling may have occurred via vDB. Furthermore, the vDB-ventral CA3 projection tends to be lateralized *(S24)*, which is consistent with the heavier labeling we observed in ipsilateral ventral CA3 at 48 h post-injection. It is more difficult to speculate on how PRV virions were retrogradely transported to intermediate CA3, because its current boundaries have been only recently delineated *(S6, S25)*. Recall that we examined the number PRV (+) neurons in LS at 36 h post-injection, a time-point prior to PRV labeling in hippocampus. The rostral- and caudal-intermediate LS had fewer PRV (+) neurons at 36 h post-VTA injection than cd-LS, but more than ventral LS (Fig. 1D). It is possible that the intermediate LS neurons, together with the highly recurrent connectivity of CA3 neurons, were sufficient to account for the moderate levels of PRV (+) neurons in intermediate CA3 at 48 h post-injection. Recent reports examining the genomic architecture of the hippocampus have demonstrated that CA3 is a far more heterogeneous sub-region than previously appreciated *(S25)*. It is likely that circuit projections to VTA from intermediate and ventral CA3 may exist that are separate from the cd-LS relay circuit described here, but the complexities of these possible circuits remains to be determined.

Viability of CA3 pyramidal cells after ibotenate lesions. Because LS is in close proximity to the lateral ventricle, which could provide access of the toxin to CA3 cells, we examined the viability of dorsal CA3 neurons in cd-LS lesioned (ibotenate-microinjected) animals. There was no significant difference between the numbers of NeuN-positive dorsal CA3 pyramidal neurons in intact (688.2 ± 33.2 cells/section) vs. lesioned animals (593.8 ± 69.6; $t_{(17)} = 1.27$, $P = 0.22$). This is consistent with the hypothesis that lesion of cd-LS severed a circuit by which PRV virions were trans-synaptically and retrogradely transported to dorsal CA3 neurons from VTA via cd-LS, rather than a general loss of CA3 pyramidal cells due to non-specific effects of ibotenic acid.

Response proportions of VTA neurons to dorsal CA3 theta frequency stimulation. Overall, 86.0% (98 of 114 neurons) of all tested VTA neurons responded to theta train stimulation of dorsal CA3.

Of the 98 responsive cells, the following category proportions (24), in descending numerical order, were observed: E-E, 24.5%; I-I, 18.4%; I-N, 16.3%; E-N,16.3%; I-E, 9.2%; N-E, 8.2%; E-I, 3.1%; N-I, 2.0%, with "E" denoting excitation, "I" denoting inhibition, and "N" denoting non-responsiveness. E-E and I-I neurons were further characterized (as described in the main text) because (i) they were the two most common response types, and (ii) because they exhibited the most pronounced response (i.e., significant excitation or inhibition for at least 60 s post-stimulation) to a functionally significant input pattern (e.g., theta frequency) from the dorsal hippocampus.

Hippocampal theta frequency oscillations have long been associated with behavioral state *(S26)* and learning and memory *(S27)*. We thus chose to stimulate dorsal CA3 in a pattern that mimics its endogenous theta rhythm. However, we do not assume that VTA neuron responsivity to CA3 input is restricted only to theta rhythm; it is likely that VTA is responsive to other complex frequency patterns, but exploring this possibility is beyond the scope of the current study. An alternate approach to stimulation would have been to record spontaneous CA3 theta rhythm, and analyze the phase relationship with VTA activity. We view the stimulation and phase relation (recording) approaches as complementary, both yielding important information but neither necessarily superior to the other. As this is the first presentation of the electrophysiological properties of the CA3–LS–VTA pathway, we felt the stimulation approach is well suited for the anesthetized preparation.

Topographical characteristics of VTA responses. We also observed that VTA response patterns differed depending on the stimulating electrode placement in the dorsal hippocampal region. Most stimulation sites were in the CA3 pyramidal cell layer (PYR), the targeted area, but some stimulation sites were in CA3 stratum radiatum (SR) and fimbria (FI), areas just medial and lateral to the pyramidal cell layer, respectively (Fig. S6A). Overall, stimulation of CA3 stratum radiatum produced significantly weaker inhibition than CA3 pyramidal cell layer or fimbria stimulation (Fig. S6B; R-score: CA3-SR, 0.39 ± 0.01 *vs.* CA3-PYR, 0.28 ± 0.03 *vs.* Fimbria, 0.23 ± 0.04; ANOVA $F_{(2, 40)} = 6.26$, $P = 0.005$, Newman-Keuls *post-hoc*), although proportionally more cells were inhibited (CA3-SR, 45.2%, 14 of 31 cells *vs.* CA3-PYR, 33.9%, 21 of 62 *vs.* Fimbria, 33.3%, 7 of 21; Fisher's Exact, $P = 0.03$; Fig. S6C). When the E-E and I-I sub-groups were analyzed, inhibition was also stronger in I-I cells when the pyramidal cell layer was stimulated vs. stratum radiatum (Table S3; R-score: CA3-PYR, 0.20 ± 0.03, 9 of 18 cells *vs.* CA3-SR, 0.41 ± 0.01, 8 of 18 cells; $U_{(17)} = 6.0$, $P = 0.002$).We also found that E-E responses occurred most often when stimulation sites were in the pyramidal cell layer (66.7.0%, 16 of 24 cells), followed by the fimbria (20.1%, 5 of 24 cells), and least often for sites in the stratum radiatum (12.5%, 3 of 24 cells; Table S3). The fact that stimulation of the pyramidal cell layer and fimbria produced somewhat similar results is not surprising because the pyramidal cell axons that exit dorsal hippocampus project through the adjacent medial fimbria fiber bundle *(S28)*; the majority of our fimbria stimulations were in the medial aspect. In general, we found that compared to stimulation of the stratum radiatum, stimulation of the pyramidal cell layer or fimbria resulted in stronger inhibitory responses, and an increased number of DA cells responding with sustained excitation (E-E). These findings are consistent with our anatomical studies; both suggest that the CA3 pyramidal cell region has a functionally potent connection with the VTA. We made a concerted effort to record from most regions of VTA, and used a 10º recording position to access medial portions of VTA, an area often missed when a 0º position is used. We found responsive neurons throughout the VTA, and there were no obvious "hot" spots for finding these neurons.

Chemical stimulation of dorsal CA3. Microinjection of D, L-homocysteic acid (DLH) was used to chemically stimulate dorsal CA3 to test whether results obtained using electrical stimulation were in part, mediated through activation of fibers of passage. For this, we first optimized the DLH microinjection protocol to ensure reliable CA3 pyramidal neurons activation over the entire drug infusion period ($n = 9$ cells; 4 animals). Picospritzer-aided microinjections with inter-pulse intervals of 3.0 s or less quickly resulted in apparent depolarization block (Fig. S7A), and was therefore an inadequate protocol for reliable chemical activation of CA3 pyramidal neurons. However, 4.0 s was a sufficiently long inter-pulse interval to consistently evoked CA3 pyramidal neuron responses (Fig. S7B). Using this 4.0 s inter-pulse interval protocol, we found that 60 nl of 1.0 mM DLH infused over 160 s elicited long-

lasting excitation or inhibition in VTA neurons (Fig. S7C). The vast majority of VTA neurons responded to such chemical stimulation (85.7%, 36 of 42 cells; 10 animals), with approximately equal numbers of excited (55.6%, 20 of 36) and inhibited neurons (44.4%, 16 of 36). Both responses persisted for as long as stable recordings could be maintained for the majority of cells (at 9 min post-DLH: excited, 15 of 20 initially responding cells; inhibited, 10 of 16 initially responding cells). The firing rates (60 s bins) of excited cells were significantly elevated from 3 to 9 min post-infusion (Fig. S7C; mean base firing rate, 4.0 spikes/s *vs.* mean excitation firing rate, 5.4 spikes/s; Range: 31.0 – 47.4% above baseline; repeated ANOVA $F_{(9, 20)} = 55.1$, $P = 0.0003$, Dunnett's post-hoc). The firing rates of inhibited cells were significantly reduced from 4 to 9 min post-infusion (mean base firing rate, 4.2 spikes/s *vs.* mean inhibition firing rate, 3.3 spikes/s; Range: 18.3 – 24% below baseline; repeated ANOVA $F_{(9, 16)} = 46.9$, $P = 0.00008$, Dunnett's *post-hoc*). The small amount of DLH (60 nl) that was microinjected into a structure as large of as hippocampus, and the high proportion of responsive VTA neurons, reinforces our hypothesis that the dorsal CA3–cd-LS–VTA pathway is a robust functional circuit.

Single pulse stimulation of E-E and I-I neurons. Recall that I-I and E-E neuron categories were based on responses to theta frequency electrical stimulation. In additional to theta stimulation, we also examined I-I and E-E neuron responses to single-pulse stimulation of dorsal CA3 *(S29)*. Latency to response for I-I (non-DA) neurons preceded E-E (DA) neurons (Table S1; non-DA inhibition latency, 51.4 ± 13.9 ms *vs.* DA excitation latency, 159.6 ± 35.8 ms). This led us to hypothesize that VTA DA neuron excitation in response to CA3 theta stimulation was due to disinhibition; local VTA GABA neuron which normally hold DA neuron under tonic inhibition no longer do so, and thus disinhibited DA neurons. As described in the main text, we tested our hypothesis with local application GABA receptor antagonists, which blocked responses to the theta stimulation (Fig. 3).

Single pulse stimulation of all recorded neurons. When possible, all recorded VTA neurons were tested with single-pulse stimulation of dorsal CA3. Within this pooled population of cells, which included I-I and E-E neurons, 62.3% (48 of 76 cells; 32 animals) responded to single-pulse stimulation (0.5 mA, 0.3 ms pulses) of the dorsal CA3 (Table S2). Putative DA neurons *(S29)* predominantly responded to dorsal CA3 with inhibition (45.5%; 25 of 55 cells), although a number of them were also excited (25.5%; 14 of 55 cells) or non-responsive (29.1%; 16 of 55 cells). Interestingly, most putative GABA neurons were non-responsive (57.1%; 12 of 21 cells), with all but one neuron showing inhibition (88.9%; 8 of 9 cells). Response latencies overlapped and varied widely for cell and response types, but DA excitatory responses were much shorter in duration than inhibitory responses (93.2 ± 27.0 msec *vs.* 288.4 ± 39.4 msec; $U_{(38)} = 48.5$, $P = 0.0002$; Table S2).

Effect of GABA microinjections in LS on responses to single-pulse stimulation. Recall that we transiently inactivated cd-LS with a local microinjection of GABA to test the role of cd-LS in VTA neuron responses to dorsal CA3 stimulation. Microinjection of GABA in cd-LS blocked the excitatory response to single-pulse stimulation (Fig. S8A; R-mag: +49.8 ± 10.5 *vs*. -4.3 ± 6.3; repeated ANOVA $F_{(2, 5)} = 23.43$, $P = 0.006$; Newman-Keuls *post-hoc*, $P = 0.008$), which was later fully recovered (R-mag: +49.9 ± 14.7; *post-hoc*, $P = 0.005$). Similarly, inhibitory responses were also blocked (Fig. S8A; R-mag: -44.6 ± 8.7 *vs.* +4.6 ± 6.7; repeated ANOVA $F_{(2, 9)} = 8.06$, $P = 0.008$; Newman-Keuls *post-hoc*, $P = 0.007$), and later recovered (R-mag: -26.7 ± 11.6; *post-hoc*, $P = 0.03$). Overall, all but one tested cell showed decreased responding after cd-LS inactivation. The one cell that did not show decreased responding showed the opposite response after cd-LS inactivation; that is, its baseline response was inhibitory and after cd-LS inactivation, its response to single-pulse stimulation was excitatory.

Effect of GABA microinjections in LS on cd-LS function. GABA infusions did not seem to compromise the integrity of cd-LS, as we were able to replicate blockade and recovery profiles on multiple neurons during a day's recording session. In general, we found that the maximal response blockade occurred 3-5 min. after drug infusion. Responses typically recovered 10-15 min. after drug infusion. Vehicle (aCSF) microinjection in cd-LS ($n = 3$ animals) had no effect on VTA responses to CA3 stimulation ($t_{(5)} = 0.54$, $P = 0.62$). Similarly, GABA microinjections into the lateral ventricle ($n = 4$ animals) had no significant effect on VTA responses to CA3 stimulation ($t_{(5)} = 0.44$, $P = 0.68$).

Effect of picrotoxin-CGP microinjection on VTA responses to single-pulse stimulation. Recall that we locally microinjected a mixture of picrotoxin and CGP 55845 antagonists near the recorded VTA neuron using a double-barrel ejection and recording pipette to test whether responses were GABA receptor dependent (n = 7 animals). The majority of tested neurons were putative DA neurons since almost all putative GABA neurons were unresponsive to single-pulse stimulation (Table S2). This GABA receptor antagonist treatment blocked VTA neural excitation by dorsal CA3 stimulation (Fig. S8B; R-mag: pre, +37.3 ± 6.4 *vs.* post, +6.8 ± 7.9, paired $t_{(5)} = 3.7$, $P = 0.02$), indicating that this excitation may be due to a disinhibitory effect similar to that found for CA3 theta stimulation. Interestingly, inhibition of VTA neurons by single-pulse CA3 stimulation was not significantly affected by local microinjection of the GABA receptor antagonist mixture (R-mag: pre, -65.5 ± 5.8 *vs.* post, -60.2 ± 12.6, paired $t_{(8)} = 3.7$, $P = 0.59$. It is currently unknown what caused the inhibitory response to single-pulse stimulation in these DA neurons, but studies have shown that metabotropic glutamate-1 receptors *(S30)*, and other G-protein coupled receptors can inhibit DA neurons. Future experiments are needed to address possible mechanisms.

Effect of picrotoxin-CGP on baseline firing rates. Combined blockade of GABA-A and GABA-B receptors alone increased basal firing rates of VTA neurons. The baseline firing rate of excited cells increased from 3.6 ± 0.9 to 7.6 ± 1.1 spikes/sec ($t_{(4)} = 6.1$, $P = 0.004$). This raises the possibility that the attenuated excitations to CA3 stimulation after drug application were confounded by a physiological ceiling in DA neuron firing capabilities. However, under GABA receptor blockade, post-theta stimulation firing rates still increased (to 8.6 ± 1.8 spikes/sec) during the early epoch. Using photic stimulation of channelrhodopsin-transduced VTA DA neurons, a previous study found that DA neurons could reliably follow train stimulation at 10Hz, and that spike entrainment began to decline at 20Hz *(S31)*, a rate far faster than that in our current study. Their results show that the firing rates we observed were physiological possible for DA neurons to maintain, and argues against a ceiling effect confound in our GABA receptor antagonism experiments.

Effect of dorsal CA3 misses with B-M microinjection on context-induced reinstatement behavior. Recall that we used an ABA design to establish context-induced reinstatement of cocaine-seeking *(S29)*. Although bilateral injections of B-M in dorsal CA3 blocked reinstatement of lever-pressing upon re-exposure to the cocaine-paired environment (Fig. 4A), animals with at least one intact CA3 (i.e., dorsal CA3 misses of B-M injection on at least one-side; $n = 9$) showed preserved reinstatement of cocaine-seeking (CA3 miss during reinstatement test, 43.5 ± 11.1 *vs.* last extinction test, 15.2 ± 5.6/2h; repeated measures ANOVA, $F_{(3,24)} = 4.756$, $P = 0.01$, Bonferroni *post hoc*, $P = 0.03$). This indicates that bilateral inactivation of CA3, and not adjacent areas, is required to block the context-induced reinstatement of cocaine-seeking.

Previous studies have shown that inactivation of dorsal hippocampus prevents context-induced cocaine seeking *(S19, S32)*. Although these studies did not specifically target CA3, it is possible that the solutions in those injections diffused into dorsal CA3 to elicit effects on context-induced drug seeking. Another possibility could be that both CA1 and CA3 subfields are involved.

Inactive lever-pressing during reinstatement testing and the effect of intracranial baclofen-muscimol injections on locomotor activity. To rule out possible effects of intracranial infusions on motor activity, locomotor tests were conducted using an open field apparatus (2 h) in different groups of rats for CA3 *vs.* LS-VTA. Administration of B-M (baclofen, 1.0mM; muscimol, 0.1mM) into CA3 bilaterally, did not affect either horizontal (Paired *t*-test: $t_{(4)} = 1.073$, $P = 0.3437$) or total (Paired *t*-test: $t_{(4)} = 0.5890$, $P = 0.5875$) locomotion compared to aCSF injections. Therefore, the non-specific reduction of inactive lever presses during reinstatement cannot be attributed to a general motor effect of treatments. In contrast, this same concentration of B-M in our contralateral LS-VTA experiments reduced locomotor activity, and we found this was due to effects in VTA, rather than in LS. Specifically, we found that lowering the concentration of B-M in VTA (baclofen, 0.1 mM; muscimol, 0.01 mM), while maintaining the original concentration of B-M in LS, did not affect either horizontal or total locomotor activity of rats compared to aCSF (Paired *t*-test: $t_{(5)} = -0.194$ and 0.250, $P = 0.854$ and 0.812, respectively). Therefore, these optimized concentrations of B-M were used in our VTA-LS contralateral reinstatement tests.

cd-LS in the dorsal CA3 to VTA pathway. The LS was the first brain region found to support intracranial self-stimulation *(S33)*, and stimulation of cd-LS supports the highest rates of lever pressing and lowest current thresholds of all LS regions *(S34)*. Our results using a contralateral disconnection approach further implicate cd-LS in reward-seeking, and demonstrate that cd-LS and VTA act in conjunction to regulate context-induced reinstatement of extinguished cocaine seeking. The VTA receives inputs from numerous brain nuclei, but the LS projection to VTA has received little attention, perhaps because LS was not recognized as a substantial VTA afferent until recently *(S22)*.

Supplementary Figures

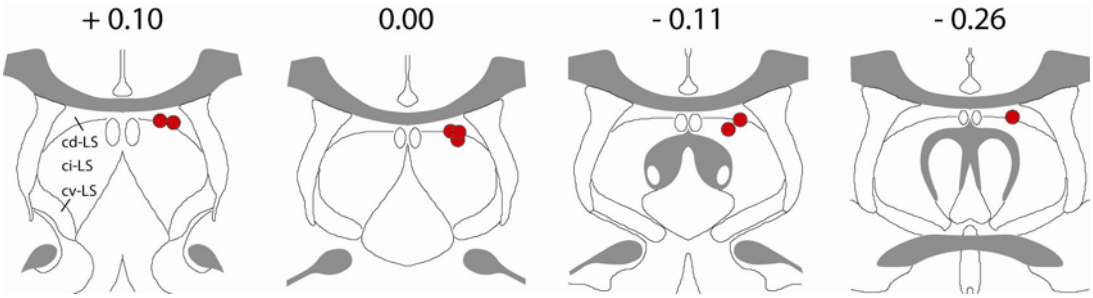

Fig. S1. Schematic plots of cd-LS inactivation sites for electrophysiological studies. GABA was injected to inactivate cd-LS after baseline responses to dorsal CA3 theta frequency or single-pulse stimulation were established. Numbers indicate distance (mm) from bregma. cd-LS, caudodorsal lateral septum; ci-LS, caudointermediate lateral septum; cv-LS, caudoventral lateral septum. Maps adapted from Swanson (2003).

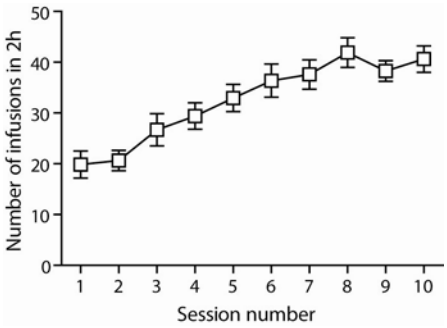

Fig. S2. Acquisition curve for cocaine self-administration. Mean ± SEM cocaine infusions in the 10, 2 h-long sessions over which animals met criteria for self-administration (10 sessions with > 10 infusions/session). Extinction training the alternative context began after these 10 sessions were completed.

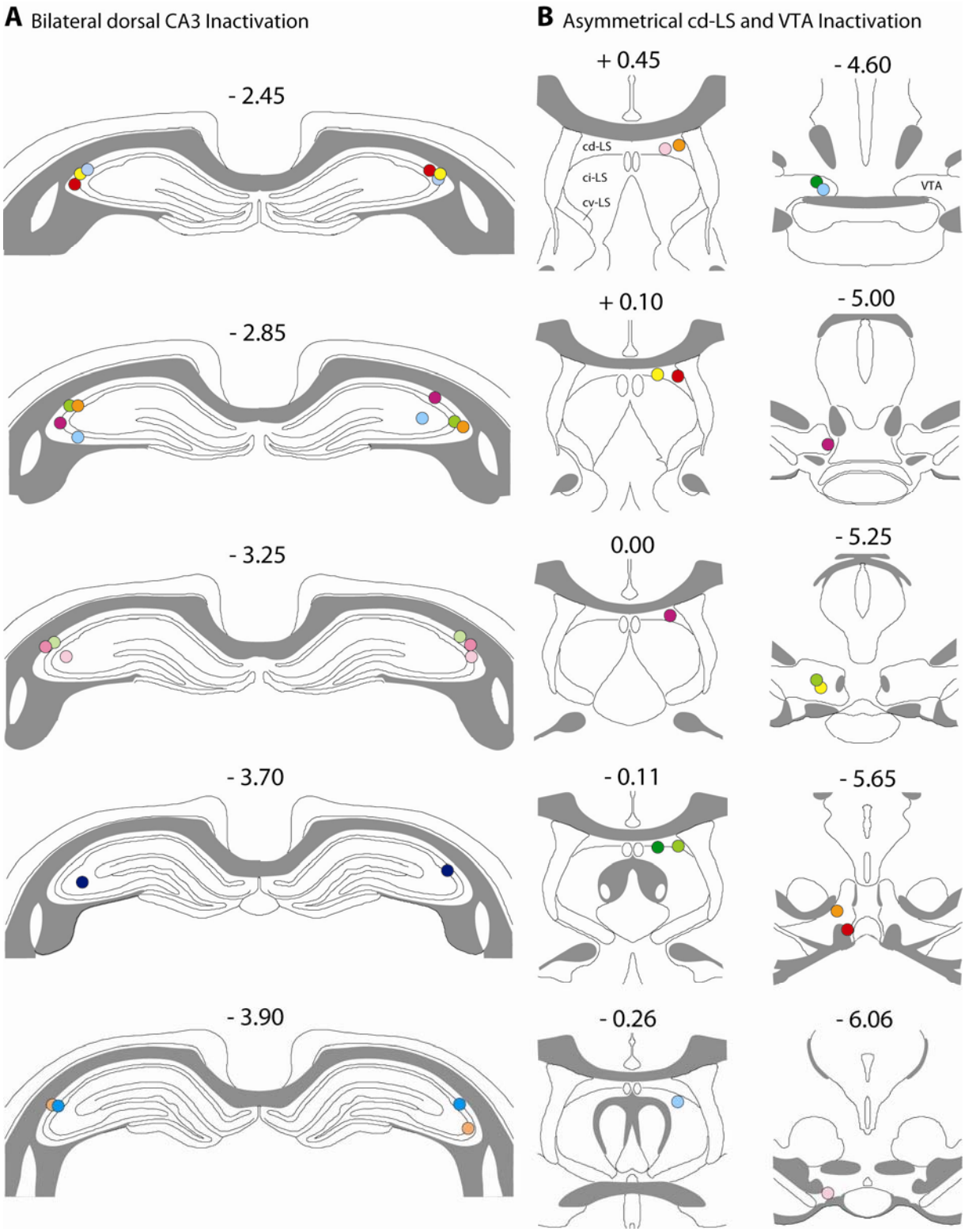

Fig. S3. Schematic plots of inactivation sites for behavioral studies. (**A**) Dorsal CA3 was bilaterally inactivated with an injection of baclofen-muscimol (B-M) in animals 5 min prior to the testing for context-induced reinstatement of cocaine-seeking. Same colored dots on the map refer to injections in each hemisphere from the same animal. (**B**) A disconnect strategy was performed by placing a unilateral

injection of baclofen-muscimol (B-M) in cd-LS with an injection of B-M placed in the contralateral VTA prior to reinstatement testing. Same colored dots on cd-LS and VTA maps refer to injection sites in the same animal. Maps adapted from Swanson (2003).

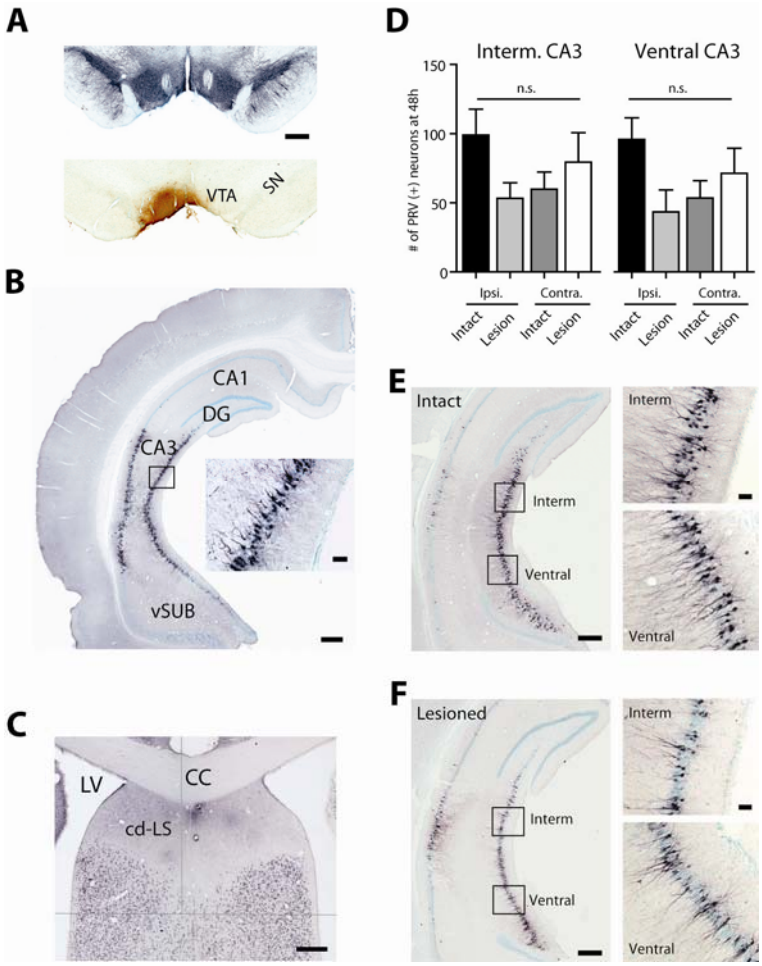

Fig. S4. Intermediate and ventral CA3: PRV labeling and effects of cd-LS lesions. (**A**) Photomicrographs of VTA sections near the PRV injection site from the same brain, processed for tyrosine hydroxylase (TH) immunoreactivity (upper; blue-grey reaction product) or for cholera toxin subunit b (CTb) immunoreactivity (lower; brown reaction product) (**B**) Photomicrographs of PRV immunoreactivity (black-purple reaction product) in rostral intermediate hippocampus 48 h following PRV injection in VTA. Inset image is a higher-power magnification of area delineated by the rectangle in the larger image. (**C**) Merged photomicrograph of NeuN immunoreactivity (black-purple reaction product) in LS from cd-LS lesioned animals. Grey lines delineate boundaries of individual photomicrographs. (**D**) Cell counts of PRV (+) CA3 pyramidal cells in intermediate and ventral CA3 from intact and cd-LS lesioned animals. n.s., non-significant differences. (**E**) Left: Representative photomicrograph from caudal hippocampus in an intact animal. Right: The two photomicrographs are higher-power photomicrographs of intermediate CA3 (upper) and ventral CA3 (lower) delineated by the upper and lower rectangles in the larger image to the left, respectively. (**F**) Left: Representative photomicrograph from caudal hippocampus in an cd-LS lesioned animal. Right: The two photomicrographs are higher-power photomicrographs of intermediate CA3 (upper) and ventral CA3 (lower) delineated by the upper and lower rectangles in the larger image to the left, respectively. The hemisphere ipsilateral to the PRV injection site in VTA is shown in all photomicrographs in which only one hemisphere is shown. Dorsal is up for all panels. All images were

obtained from coronal tissue sections. Contra., contralateral; CC, corpus callosum; cd-LS, caudodorsal lateral septum; DG, dentate gyrus; Interm, intermediate CA3; Ipsi., ipsilateral; LV, lateral ventricle; SN, substania nigra; Ventral, ventral CA3; VTA, ventral tegmental area; VSUB, ventral subiculum. Scale bars: S4A and S4C = 250µm, S4B, S4E (left, upper and lower) = 500µm; S4B (inset), S4E (right, both photomicrographs) = 50µm.

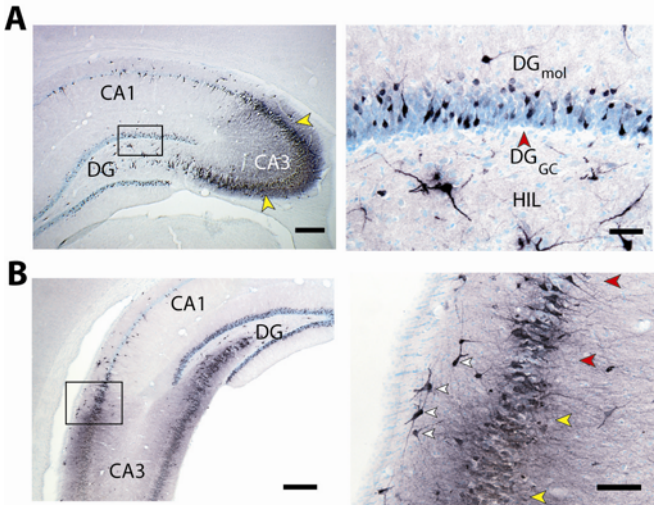

Fig. S5. PRV labeling in dorsal and intermediate hippocampus at 60 h post-PRV injection in VTA. (**A**) Photomicrographs of dorsal hippocampus. Left: Region between yellow arrowheads delineate region of necrotic-like CA3 pyramidal cells. Right: Higher-power magnification PRV labeling in dentate gyrus, the area delineated by the rectangle in left image. (**B**) Photomicrographs of intermediate hippocampus. As with dorsal hippocampus, intermediate hippocampus also exhibited regions of necrotic-like neurons. Right image is a higher-power magnification of area delineated by rectangle in left image. Right: Region between yellow arrowheads delineate region where necrotic-like intermediate CA3 pyramidal neurons (see also S5A, left) were often observed adjacent to labeled, but structurally intact pyramidal cells (region between red arrowheads). White arrowheads point to stratum oriens horizontal interneurons. The hemisphere ipsilateral to the PRV injection in VTA is shown in all photomicrographs. Dorsal is up for all panels. All images were obtained from coronally cut tissue sections. DG, dentate gyrus; DGmol, dentate gyrus molecular layer; DGGC, dentate gyrus granule cell layer; HIL, hillus. Scale bars: S5A (left) and S5B (left) = 250µm, S5A (right) and S5B (right) = 50µm.

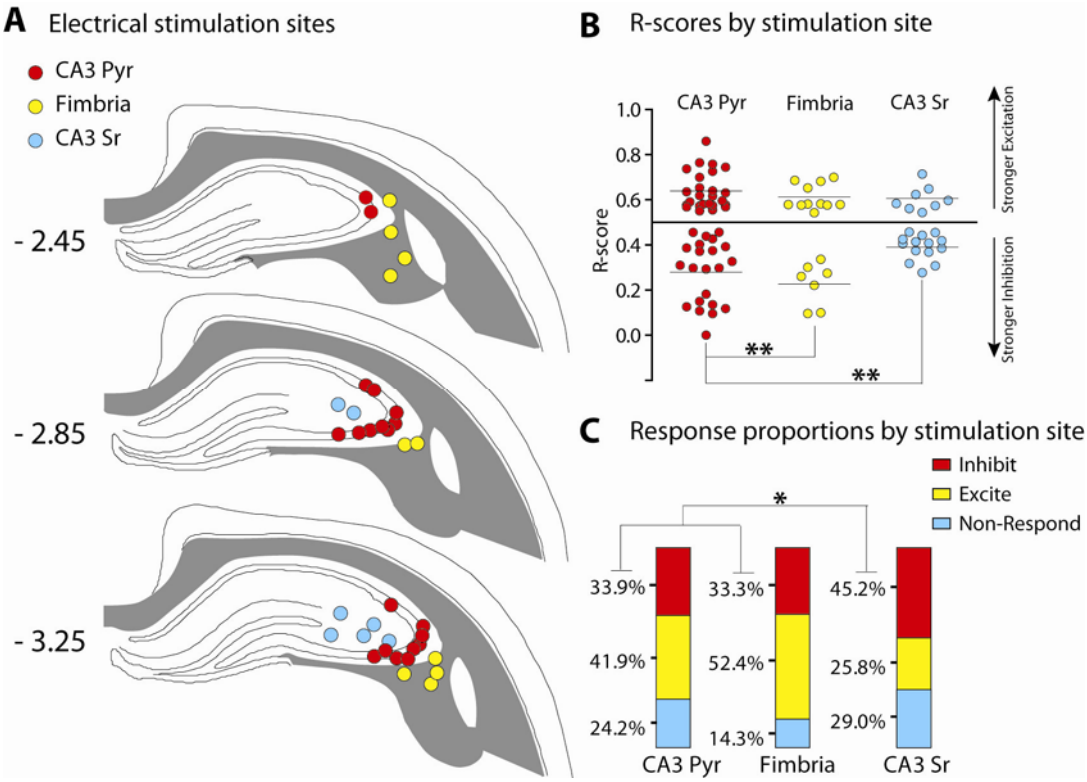

Fig. S6. VTA neuron responses to theta frequency stimulation as a function of electrical stimulation sites in sub-regions of dorsal hippocampus. (**A**) Schematic plots of electrical stimulation sites. Numbers indicate distance (mm) from bregma. (**B**) VTA neuron responsivity (R-scores) to theta frequency stimulation in differing dorsal hippocampal sub-regions (** $P = 0.005$) (**C**) Proportion of inhibited, excited and non-responsive neurons (* $P = 0.03$; Fisher Exact). CA3 Pyr, CA3 pyramidal cell layer; CA3 Sr, CA3 stratum radiatum. Maps adapted from Swanson (2003).

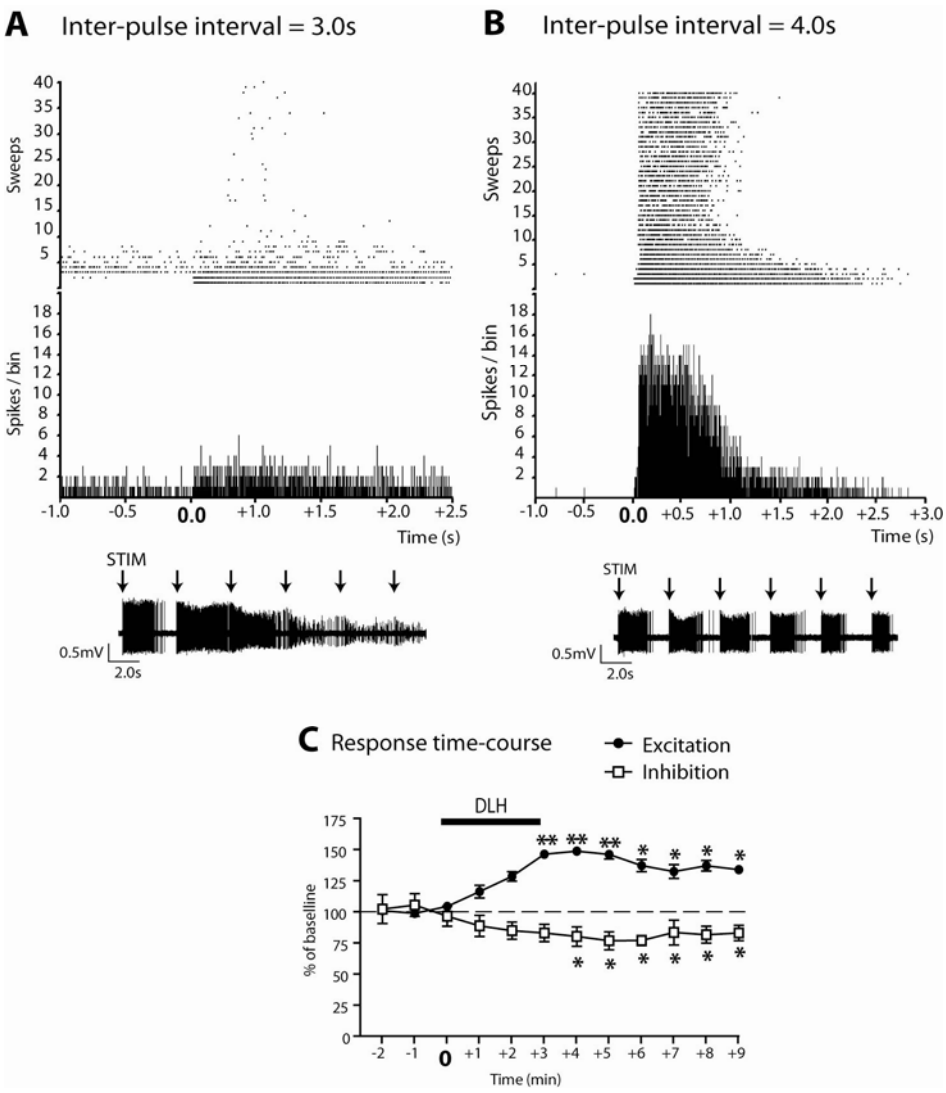

Fig. S7. Chemical stimulation of dorsal CA3 with D, L-.homocysteic acid. (**A**) Peri-stimulus time histograms, raster plots, and spike trains of CA3 pyramidal cell recordings during locally applied D, L-homocysteic acid (DLH) at three-second inter-pulse intervals. (**B**) Same as in (A) except with four-second inter-pulse intervals. Dorsal CA3 pyramidal neurons would reliably follow chemical stimulation by DLH with inter-pulse intervals of 4.0 s, but not ≤ 3.0s. (**C**) Time-course of VTA responses to CA3 stimulation by DLH (* $P < 0.05$, ** $P < 0.01$).

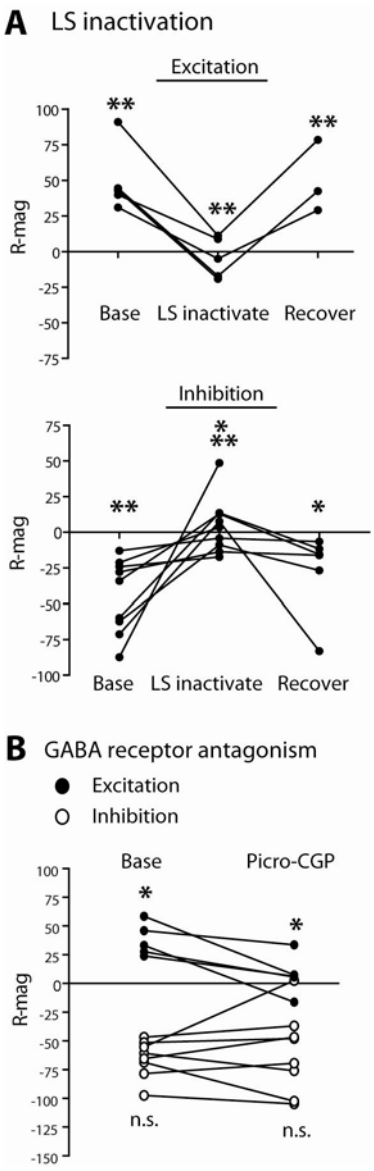

Fig. S8. Effect of cd-LS inactivation and local GABA receptor blockade on VTA responses to single-pulse stimulation. (**A**) Response magnitudes (R-mag) for excited (upper) or inhibited (lower) VTA cells to dorsal CA3single-pulse stimulation, before, during, and after cd-LS was inactivated by a GABA microinjection (* $P < 0.05$, ** $P < 0.01$). Inactivation of LS blocked excitatory and inhibitory responses to theta frequency stimulation. (**B**) R-mags for excited and inhibited VTA cells to single-pulse stimulation, before and after picrotoxin-CGP 55845 was locally microinfused near the recorded VTA neuron. The mixture of GABA receptor antagonists each blocked excitatory (* $P = 0.02$), but not inhibitory responses. GABA-R, GABA receptor; n.s, not significant.

		I-I (non-DA)	E-E (DA)
Cell Properties	**Number of neurons**	18	24
	Baseline firing rate (spikes/s)	13.0 ± 2.0	3.9 ± 0.4
	Spike time to negative trough (ms)	0.95 ± .08	1.32 ± 0.04
Theta Train	**R-Score**	0.29 ± 0.03	0.63 ± 0.01
	Rate (spike/sec): pre-stim	12.2 ± 1.5**	3.6± 0.4***
	Rate (spike/sec): post-stim	8.3 ± 1.4**	5.2 ± 0.5***
	coefficient of variation: pre-stim	0.52 ± .05	0.49 ± .05**
	coefficient of variation: post-stim	0.64 ± .09	0.61 ± .07**
	% of spikes in burst: pre-stim	N.D.	4.7 ± 1.8***
	% of spikes in burst: post-stim	N.D.	15.8 ± 4.0***
Single Pulse	**Excite: Latency to response (ms)**	34.9†	159.6 ± 35.8*
	Excite: Response duration (ms)	45.0†	79.0 ± 21.3
	Excite: Response magnitude	36.9†	35.7 ± 2.8
	Inhibit: Latency to response (ms)	51.4 ± 13.9*	183.2 ± 54.0
	Inhibit: Response duration (ms)	259.2 ± 73.4	287.8 ± 66.2
	Inhibit: Response magnitude	-72.1 ± 30.5	-47.7 ± 17.4

Table S1. Summary of cell characteristics and response properties for E-E (DA) and I-I (non-DA) neurons to theta train and single pulse stimulation. All values are means ± SEM. R-Scores were calculated for the early epoch (0-5 s post-stimulation). Pre- and post-stimulation numbers for rate, coefficient of variation and % of spikes in burst were calculated for the late epoch (5-60 s post-stimulation). Only some comparisons are highlighted, notably between pre- and post-stimulation values within the same cell type (i.e., within same table column) under the "Theta Train" section, and between single-pulse excitation in E-E cells and single-pulse inhibition in I-I cells under the "Single Pulse" section. Therefore, the symbols do not reflect all possible significant differences among values in the table. †No variance because only non-DA cell was excited. N.D., not determined. *, $P < 0.05$; **, $P < 0.01$; ***, $P < 0.001$; Student's *t*-test.

		I-I (non-DA)	E-E (DA)
CA3-Pyr.	**% of cells**	50.0 (9)	68.0 (16)
	R-score	0.20 ± 0.03 **	0.64 ± 0.01
Fimbria	**% of cells**	5.6 (1)	20.0 (5)
	R-score	0.10 (82.1%)	0.64 ± 0.01
CA3-SR	**% of cells**	44.4 (8)	12.0 (3)
	R-score	0.41 ± 0.01**	0.62 ± 0.02

Table S3. Summary of VTA neurons responses to theta train stimulation by topographical location of stimulation in hippocampus. All values are means ± SEM. Numbers in parentheses in "% of cells" rows correspond to number of neurons. R-scores from 0.5 to 1.0 indicate increasing magnitudes of excitation. R-scores from 0.5 to 0.0 indicate increasing magnitudes of inhibition *(S24)*. CA3-Pyr., CA3 pyramidal cell layer; CA3-SR,, CA3 stratum radiatum; **, $P < 0.01$; Mann-Whitney test. Because only one I-I neuron responded to fimbria stimulation, it was excluded for Response Score comparisons.

References and Notes

1. P. N. Tobler, C. D. Fiorillo, W. Schultz, Adaptive coding of reward value by dopamine neurons. *Science* **307**, 1642 (2005). doi:10.1126/science.1105370 Medline

2. H. Eichenbaum, Cognitive processes and neural representations that underlie declarative memory. *Neuron* **44**, 109 (2004). doi:10.1016/j.neuron.2004.08.028 Medline

3. J. E. Lisman, A. A. Grace, The hippocampal-VTA loop: Controlling the entry of information into long-term memory. *Neuron* **46**, 703 (2005). doi:10.1016/j.neuron.2005.05.002 Medline

4. J. P. Card *et al*., Pseudorabies virus infection of the rat central nervous system: Ultrastructural characterization of viral replication, transport, and pathogenesis. *J. Neurosci.* **13**, 2515 (1993). Medline

5. For simplicity, the region containing CA2 and CA3 will be referred to as CA3.

6. A. H. Luo, G. Aston-Jones, Circuit projection from suprachiasmatic nucleus to ventral tegmental area: A novel circadian output pathway. *Eur. J. Neurosci.* **29**, 748 (2009). doi:10.1111/j.1460-9568.2008.06606.x Medline

7. M. Legault, P. P. Rompré, R. A. Wise, Chemical stimulation of the ventral hippocampus elevates nucleus accumbens dopamine by activating dopaminergic neurons of the ventral tegmental area. *J. Neurosci.* **20**, 1635 (2000). Medline

8. S. B. Floresco, C. L. Todd, A. A. Grace, Glutamatergic afferents from the hippocampus to the nucleus accumbens regulate activity of ventral tegmental area dopamine neurons. *J. Neurosci.* **21**, 4915 (2001). Medline

9. L. W. Swanson, P. E. Sawchenko, W. M. Cowan, Evidence for collateral projections by neurons in Ammon's horn, the dentate gyrus, and the subiculum: A multiple retrograde labeling study in the rat. *J. Neurosci.* **1**, 548 (1981). Medline

10. M. E. Hasselmo, What is the function of hippocampal theta rhythm?—Linking behavioral data to phasic properties of field potential and unit recording data. *Hippocampus* **15**, 936 (2005). doi:10.1002/hipo.20116 Medline

11. Materials and methods are available as supporting material on *Science* Online.

12. S. W. Johnson, R. A. North, Opioids excite dopamine neurons by hyperpolarization of local interneurons. *J. Neurosci.* **12**, 483 (1992). Medline

13. R. A. Fuchs, J. L. Eaddy, Z. I. Su, G. H. Bell, Interactions of the basolateral amygdala with the dorsal hippocampus and dorsomedial prefrontal cortex regulate drug context-induced reinstatement of cocaine-seeking in rats. *Eur. J. Neurosci.* **26**, 487 (2007). doi:10.1111/j.1460-9568.2007.05674.x Medline

14. S. R. Vorel, X. Liu, R. J. Hayes, J. A. Spector, E. L. Gardner, Relapse to cocaine-seeking after hippocampal theta burst stimulation. *Science* **292**, 1175 (2001). doi:10.1126/science.1058043 Medline

15. J. M. Bossert, U. E. Ghitza, L. Lu, D. H. Epstein, Y. Shaham, Neurobiology of relapse to heroin and cocaine seeking: An update and clinical implications. *Eur. J. Pharmacol.* **526**, 36 (2005). doi:10.1016/j.ejphar.2005.09.030 Medline

16. J. F. DeFrance, S. T. Kitai, T. Shimono, Electrophysiological analysis of the hippocampal-septal projections. I. Response and topographical characteristics. *Exp. Brain Res.* **17**, 447 (1973). Medline

17. A. Alvernhe, T. Van Cauter, E. Save, B. Poucet, Different CA1 and CA3 representations of novel routes in a shortcut situation. *J. Neurosci.* **28**, 7324 (2008). doi:10.1523/JNEUROSCI.1909-08.2008 Medline

18. E. S. Bromberg-Martin, M. Matsumoto, O. Hikosaka, Dopamine in motivational control: Rewarding, aversive, and alerting. *Neuron* **68**, 815 (2010). doi:10.1016/j.neuron.2010.11.022 Medline

19. S. Geisler, D. S. Zahm, Afferents of the ventral tegmental area in the rat-anatomical substratum for integrative functions. *J. Comp. Neurol.* **490**, 270 (2005). doi:10.1002/cne.20668 Medline

Supporting References and Notes

S1. G. Aston-Jones, S. Chen, Y. Zhu, M. L. Oshinsky, A neural circuit for circadian regulation of arousal. *Nat. Neurosci.* **4**, 732 (2001). doi:10.1038/89522 Medline

S2. P. O'Donnell, A. Lavín, L. W. Enquist, A. A. Grace, J. P. Card, Interconnected parallel circuits between rat nucleus accumbens and thalamus revealed by retrograde transynaptic transport of pseudorabies virus. *J. Neurosci.* **17**, 2143 (1997). Medline

S3. A. H. Luo, G. Aston-Jones, Circuit projection from suprachiasmatic nucleus to ventral tegmental area: a novel circadian output pathway. *Eur. J. Neurosci.* **29**, 748 (2009). doi:10.1111/j.1460-9568.2008.06606.x Medline

S4. J. P. Card *et al*., Pseudorabies virus infection of the rat central nervous system: ultrastructural characterization of viral replication, transport, and pathogenesis. *J. Neurosci.* **13**, 2515 (1993). Medline

S5. S. Chen, M. Yang, R. R. Miselis, G. Aston-Jones, Characterization of transsynaptic tracing with central application of pseudorabies virus. *Brain Res.* **838**, 171 (1999). doi:10.1016/S0006-8993(99)01680-7 Medline

S6. M. S. Fanselow, H. W. Dong, Are the dorsal and ventral hippocampus functionally distinct structures? *Neuron* **65**, 7 (2010). doi:10.1016/j.neuron.2009.11.031 Medline

S7. L. W. Swanson, W. M. Cowan, The connections of the septal region in the rat. *J. Comp. Neurol.* **186**, 621 (1979). doi:10.1002/cne.901860408 Medline

S8. E. Jodoj, C. Chiang, G. Aston-Jones, Potent excitatory influence of prefrontal cortex activity on noradrenergic locus coeruleus neurons. *Neuroscience* **83**, 63 (1998). doi:10.1016/S0306-4522(97)00372-2 Medline

S9. J. Larson, D. Wong, G. Lynch, Patterned stimulation at the theta frequency is optimal for the induction of hippocampal long-term potentiation. *Brain Res.* **368**, 347 (1986). doi:10.1016/0006-8993(86)90579-2 Medline

S10. Y. J. Greenstein, C. Pavlides, J. Winson, Long-term potentiation in the dentate gyrus is preferentially induced at theta rhythm periodicity. *Brain Res.* **438**, 331 (1988). doi:10.1016/0006-8993(88)91358-3 Medline

S11. F. Georges, G. Aston-Jones, Activation of ventral tegmental area cells by the bed nucleus of the stria terminalis: a novel excitatory amino acid input to midbrain dopamine neurons. *J. Neurosci.* **22**, 5173 (2002). Medline

S12. C. A. Paladini, J. M. Tepper, GABA(A) and GABA(B) antagonists differentially affect the firing pattern of substantia nigra dopaminergic neurons in vivo. *Synapse* **32**, 165 (1999). doi:10.1002/(SICI)1098-2396(19990601)32:3<165::AID-SYN3>3.0.CO;2-N Medline

S13. A. H. Luo, F. E. Georges, G. S. Aston-Jones, Novel neurons in ventral tegmental area fire selectively during the active phase of the diurnal cycle. *Eur. J. Neurosci.* **27**, 408 (2008). doi:10.1111/j.1460-9568.2007.05985.x Medline

S14. A. A. Grace, B. S. Bunney, Intracellular and extracellular electrophysiology of nigral dopaminergic neurons—1. Identification and characterization. *Neuroscience* **10**, 301 (1983). doi:10.1016/0306-4522(83)90135-5 Medline

S15. M. A. Ungless, P. J. Magill, J. P. Bolam, Uniform inhibition of dopamine neurons in the ventral tegmental area by aversive stimuli. *Science* **303**, 2040 (2004). doi:10.1126/science.1093360 Medline

S16. J. B. Ranck, Jr., Studies on single neurons in dorsal hippocampal formation and septum in unrestrained rats. I. Behavioral correlates and firing repertoires. *Exp. Neurol.* **41**, 462 (1973). doi:10.1016/0014-4886(73)90290-2 Medline

S17. A. A. Grace, B. S. Bunney, The control of firing pattern in nigral dopamine neurons: burst firing. *J. Neurosci.* **4**, 2877 (1984). Medline

S18. R. J. Smith, P. Tahsili-Fahadan, G. Aston-Jones, Orexin/hypocretin is necessary for context-driven cocaine-seeking. *Neuropharmacology* **58**, 179 (2010). doi:10.1016/j.neuropharm.2009.06.042 Medline

S19. R. A. Fuchs, J. L. Eaddy, Z. I. Su, G. H. Bell, Interactions of the basolateral amygdala with the dorsal hippocampus and dorsomedial prefrontal cortex regulate drug context-induced reinstatement of cocaine-seeking in rats. *Eur. J. Neurosci.* **26**, 487 (2007). doi:10.1111/j.1460-9568.2007.05674.x Medline

S20. P. Ganter, P. Szücs, O. Paulsen, P. Somogyi, Properties of horizontal axo-axonic cells in stratum oriens of the hippocampal CA1 area of rats in vitro. *Hippocampus* **14**, 232 (2004). Medline doi:10.1002/hipo.10170

S21. P. Y. Risold, L. W. Swanson, Connections of the rat lateral septal complex. *Brain Res. Brain Res. Rev.* **24**, 115 (1997). doi:10.1016/S0165-0173(97)00009-X Medline

S22. S. Geisler, D. S. Zahm, Afferents of the ventral tegmental area in the rat-anatomical substratum for integrative functions. *J. Comp. Neurol.* **490**, 270 (2005). doi:10.1002/cne.20668 Medline

S23. O. T. Phillipson, Afferent projections to the ventral tegmental area of Tsai and interfascicular nucleus: a horseradish peroxidase study in the rat. *J. Comp. Neurol.* **187**, 117 (1979). doi:10.1002/cne.901870108 Medline

S24. R. P. Gaykema, J. van der Kuil, L. B. Hersh, P. G. Luiten, Patterns of direct projections from the hippocampus to the medial septum-diagonal band complex: anterograde tracing with Phaseolus vulgaris leucoagglutinin combined with immunohistochemistry of choline

acetyltransferase. *Neuroscience* **43**, 349 (1991). doi:10.1016/0306-4522(91)90299-4 Medline

S25. C. L. Thompson *et al*., Genomic anatomy of the hippocampus. *Neuron* **60**, 1010 (2008). doi:10.1016/j.neuron.2008.12.008 Medline

S26. C. H. Vanderwolf, Hippocampal electrical activity and voluntary movement in the rat. *Electroencephalogr. Clin. Neurophysiol.* **26**, 407 (1969). doi:10.1016/0013-4694(69)90092-3 Medline

S27. M. E. Hasselmo, What is the function of hippocampal theta rhythm?—Linking behavioral data to phasic properties of field potential and unit recording data. *Hippocampus* **15**, 936 (2005). doi:10.1002/hipo.20116 Medline

S28. L. W. Swanson, W. M. Cowan, An autoradiographic study of the organization of the efferent connections of the hippocampal formation in the rat. *J. Comp. Neurol.* **172**, 49 (1977). doi:10.1002/cne.901720104 Medline

S29. Materials and methods are available as supporting material on *Science* Online.

S30. C. D. Fiorillo, J. T. Williams, Cholinergic inhibition of ventral midbrain dopamine neurons. *J. Neurosci.* **20**, 7855 (2000). Medline

S31. H. C. Tsai *et al*., Phasic firing in dopaminergic neurons is sufficient for behavioral conditioning. *Science* **324**, 1080 (2009). doi:10.1126/science.1168878 Medline

S32. D. R. Ramirez *et al*., Dorsal hippocampal regulation of memory reconsolidation processes that facilitate drug context-induced cocaine-seeking behavior in rats. *Eur. J. Neurosci.* **30**, 901 (2009). doi:10.1111/j.1460-9568.2009.06889.x Medline

S33. J. Olds, P. Milner, Positive reinforcement produced by electrical stimulation of septal area and other regions of rat brain. *J. Comp. Physiol. Psychol.* **47**, 419 (1954). doi:10.1037/h0058775 Medline

S34. R. Prado-Alcala, A. Streather, R. A. Wise, Brain stimulation reward and dopamine terminal fields. II. Septal and cortical projections. *Brain Res.* **301**, 209 (1984). doi:10.1016/0006-8993(84)91089-8 Medline

S35. L. W. Swanson, *Brain Maps: Structure of the Rat Brain* (Elsevier Academic Press, New York, ed. 3, 2003).